Central Time-of-Flight Magnetic Shield Performance Studies

D.S. Carman, Jefferson Laboratory
G. Asryan, A. Alikhanyan National Science Laboratory
A. Ni, Kyungpook National University
ctof_field.tex

July 8, 2015

Abstract

This document details the performance studies and field reduction factors for the CTOF PMT magnetic shields. The studies were performed placing a complete production shield in the fringe field of the FROST superconducting solenoid in positions where the field strength and gradient were close matches to the expected fields the shield will encounter within the fringe field of the CLAS12 solenoid in Hall B.

1 Overview

The Central Time-of-Flight (CTOF) system is the CLAS12 detector used to measure the flight time of charged particles emerging from interactions in the target in the angular range from 35° to 125°. The system specifications call for an average time resolution for each counter along its full length of σ_{TOF}=60 ps. The CTOF detector surrounds the experimental target at a radial distance of 25 cm and consists of 48 92-cm-long scintillation bars having a trapezoidal cross section that form a hermetic barrel (see Fig. 1). The barrel will be positioned inside of the CLAS12 5-T superconducting solenoid magnet in Hall B. Each counter is read out via a PMT on each end through long light guides to position the field-sensitive PMTs in reduced field regions. However, even in these positions, the PMTs will reside in inhomogeneous fringe fields from the magnet at levels as large as 1 kG at the location of the upstream PMTs and as large as 400 G at the location of the downstream PMTs. In order to allow for operation of the PMTs in this environment, they must be operated within specially designed multi-layer magnetic shields.

The full details on the design of these shields can be found in Ref. [1]. The CTOF PMT magnetic shield system includes three passive layers and one active layer. The passive layers are made up of an external heavy shield made from 1008 steel, an intermediate layer composed of the ferromagnetic Hiperm-49, and an inner layer composed of the ferromagnetic Co-NETIC. With these three layers, calculations and tests of prototype shield systems showed that it was possible to reduce an external 1 kG field to below 1 G at the position

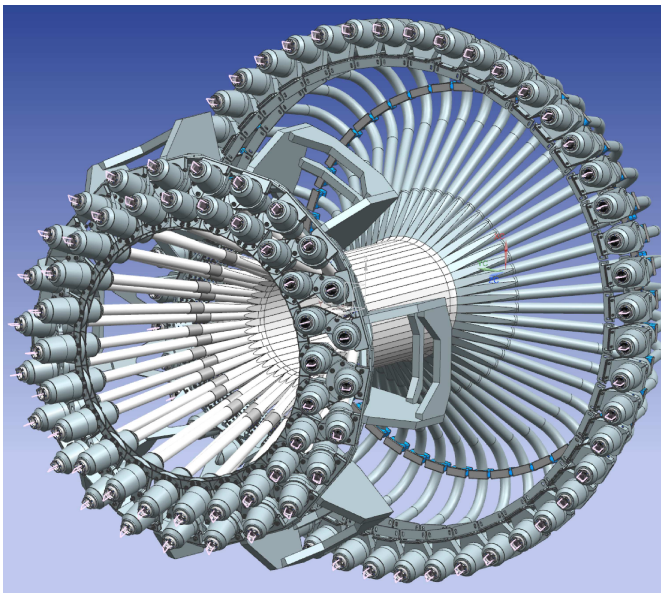

Figure 1: View of the Central Time-of-Flight (CTOF) system for CLAS12. The scintillation bars form a hermetic barrel and the PMTs are attached to the ends of long light guides. The beam enters the detector in this figure from the lower left side.

of the PMT photocathode. To reduce the field levels to below 0.5 G, which is necessary for PMT operation without loss of performance, an active shield layer is provided. The active shield consists of two sets of coils that are wrapped in two positions about a mandrel that is positioned just outside of the inner shield layer. Note that the shields for the upstream and downstream PMTs are identical in their designs.

Fig. 2 shows the results of a 3-D magnetic field calculation for the three-layer passive CTOF shield system in a 1 kG external field. The calculation plots the field profile as a function of the transverse coordinate across the shield system showing field levels below 1 G at the location of the photocathode (yellow line), the first dynode (purple line), and the middle of the accelerating structure (black line).

In the remainder of this document the results of the shield test in the FROST solenoid fringe field are presented and discussed. These tests were carried out in the period from June 8 to June 12, 2015.

2 Shield Components

Fig. 3 shows an "exploded view" assembly drawing of the CTOF PMT shield system to highlight the components that make up the different layers and their positioning with respect to each other. Note that both the external and the intermediate shield layers consist of a cylindrical section with conical endcaps. The PMT itself fits within the inner shield cylinder and the light guide feeds into the opening on the downstream end of the shield assembly. The magnetic shield design is captured in JLab assembly drawing B00000-01-04-2200. Fig. 4 shows the fully assembled shield system in a cut-away picture that shows the PMT positioned

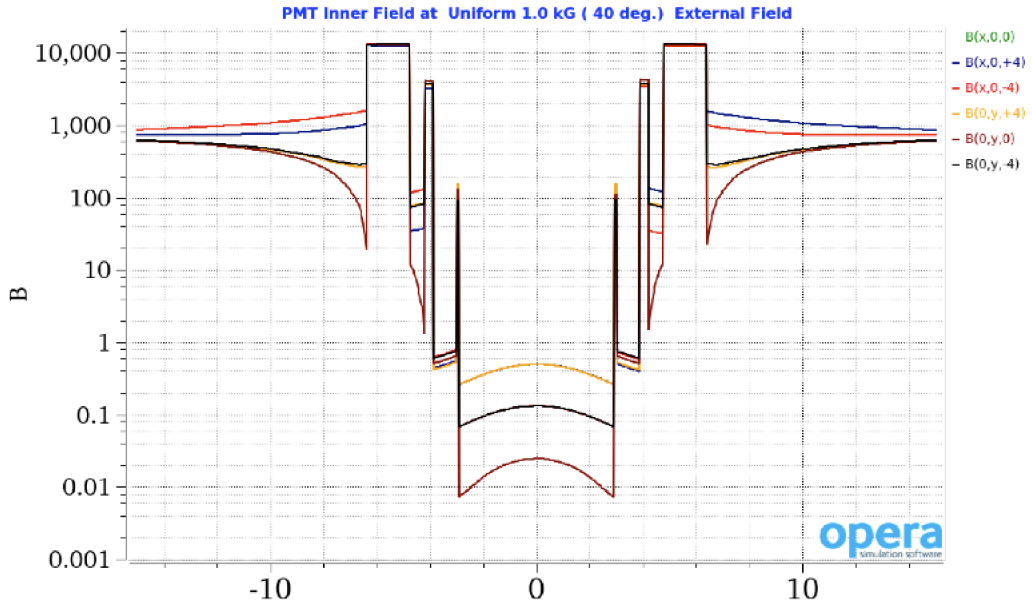

Figure 2: 3-D magnetic field calculation using the code suite Opera [2]. The calculation plots the field profile (in G) across the transverse coordinate (in cm) of the CTOF three-layer passive magnetic shield system. The different curves correspond to different transverse coordinates along the PMT (photocathode - yellow line, first dynode - purple line, middle of the accelerating structure - black line). For this calculation the external field lines were at an angle of 40° relative to the shield axis of symmetry to reflect the expected operational configuration of the shields.

within the shield. The inner shield layers are attached to the light guide using a supporting clamp and the steel shield layer is attached to a support structure secured to the CLAS12 solenoid. The weight of each shield assembly is roughly 40 lbs.

3 Shield Placement in Magnetic Field

The goal in these magnetic field tests was to place the CTOF shield in the fringe field of the FROST magnet at positions that matched the field strength and gradient the shields will see when placed in the fringe field of the CLAS12 solenoid. As shown in Fig. 1, the 48 upstream PMTs alternate in position as a function of azimuth. This is necessary to allow sufficient room for the magnetic shields. These two different versions of the CTOF counters are referred to as the “high-pitch angle” design and the “low-pitch angle” design. The tests were carried out considering both shield positions and orientations. Note that the downstream CTOF PMTs are positioned in a region of the solenoid fringe field that is a factor of two lower than for the upstream PMTs. For this reason, this configuration was not studied. All 96 magnetic shields for the CTOF PMTs are of an identical design.

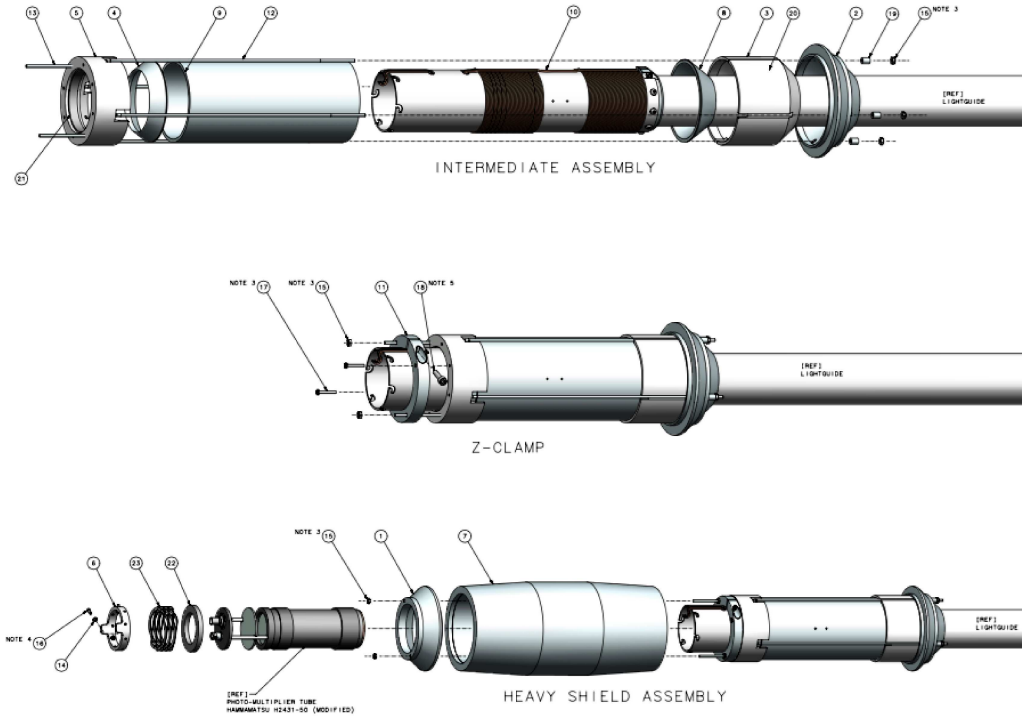

Figure 3: CTOF magnetic shield assembly drawing showing all of the components of the system and their relation to each other. Drawing ref. B00000-01-04-2200.

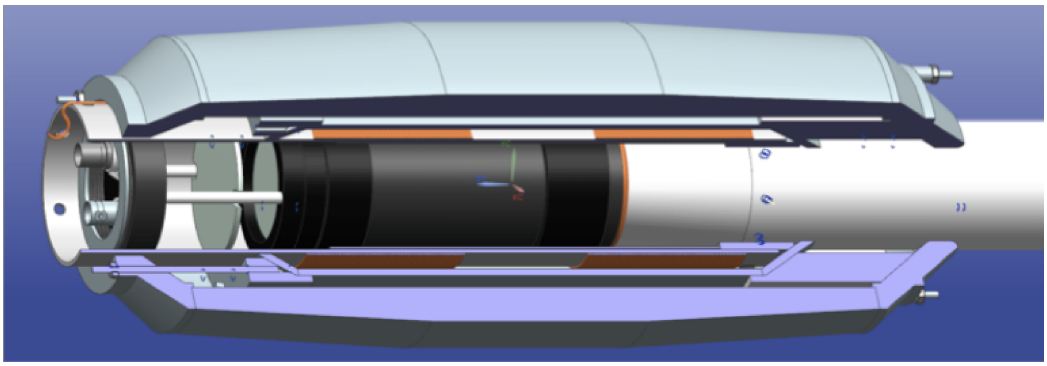

Figure 4: The CTOF shield as shown in a 3D cut-away view. The black cylinder in the middle of the shield is the PMTs. The light guide enters the shield from the right-hand side.

3.1 CLAS12 Solenoid Field

The field map of the CLAS12 5-T superconducting solenoid fringe field was provided by Renuka Rajput-Ghoshal based on a full 3D OPERA modeling of the magnet. Fig. 5 shows the position of the high-pitch angle and low-pitch angle PMTs in the CLAS12 solenoid fringe field. The fringe field was provided in the (y, z) plane in terms of (B_x, B_y, B_z) on a 10-mm grid spanning a coordinate range in the CLAS12 global coordinate system from y=0 to 1600 mm and from z=754 mm (the face of the solenoid) to 2784 mm. Here the y axis is vertical and the z axis is along the symmetry axis of the magnet. The x axis is horizontal and forms a right-handed coordinate system.

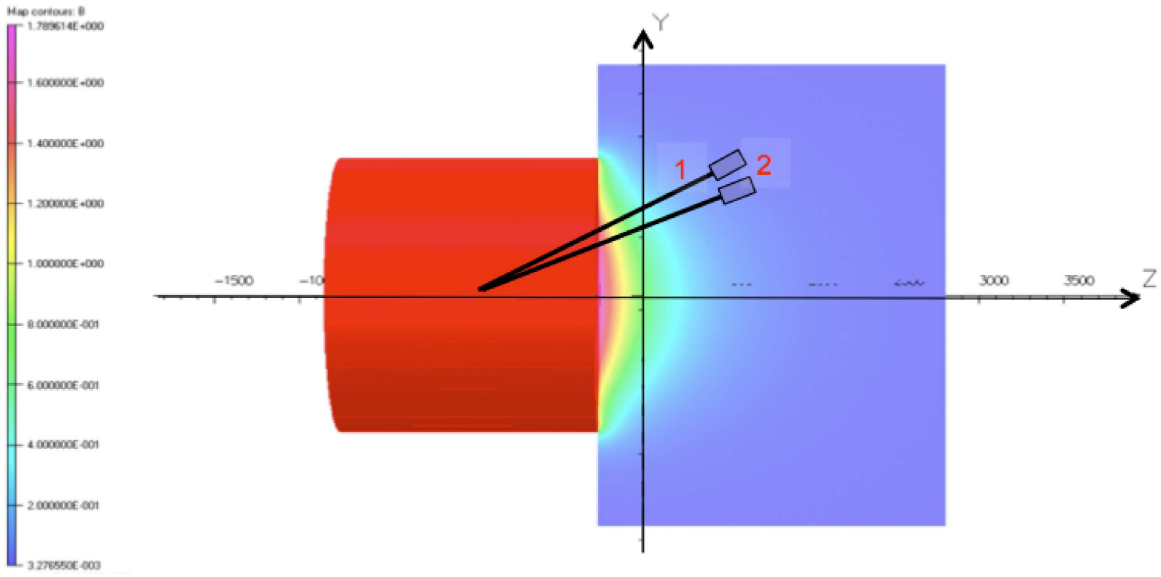

Figure 5: Output of the 3D OPERA calculation of the fringe field on one side of the CLAS12 solenoid. The figure shows the nominal locations of representative high-pitch angle and low-pitch angle CTOF PMTs in the fringe field of the magnet.

The coordinates of the two PMTs, one of the high-pitch angle design and one of the low-pitch angle design, rotated into the (y, z) plane from the CLAS12 design model, were provided by Cyril Wiggins. The provided coordinates were along the symmetry axis of the PMT at the center of the face of each steel shield cone (i.e. at the middle of the end faces of each shield). These coordinates were then matched to the closest grid point of the shield table to determine the fields relevant for the shield positioning in the FROST magnet fringe field. The (y, z) coordinates of the shields and the fields of the CLAS12 solenoid at these coordinates are given in Table 1.

In Table 1 the position labeled as "Shield End #1" is for the center of the steel cone closest to the magnet face. The position labeled as "Shield End #2" is for the center of the steel cone furthest from the magnet face. Table 1 also provides the field components in the CLAS12 solenoid fringe field at the locations of the PMT photocathode (i.e. the face of the PMT), first dynode (a distance 3 cm from the photocathode), and the middle of the accelerating structure (a distance 5.5 cm from the photocathode). All of the fields are

necessarily given without any shields present as the presence of the shields actually modifies the fringe field distribution significantly.

High-Pitch Angle Design			
	Coordinates	Magnetic Field Components	
Position	(y, z)	(B_y, B_z)	$(B_{y'}, B_{z'})$
Shield End #1	(28.53, 52.77) in	(981, 192) G	(776, 630) G
Photocathode	(31.17, 57.48) in	(612, 118) G	(485, 392) G
First Dynode	(32.63, 60.10) in	(491, 93) G	(390, 313) G
Middle Dynode	(33.84, 62.29) in	(405, 85) G	(318, 265) G
Shield End #2	(35.15, 64.64) in	(337, 78) G	(261, 227) G
Low-Pitch Angle Design			
	Coordinates	Magnetic Field Components	
Position	(y, z)	(B_y, B_z)	$(B_{y'}, B_{z'})$
Shield End #1	(24.52, 55.18) in	(956, 493) G	(702, 815) G
Photocathode	(26.53, 60.19) in	(632, 329) G	(463, 542) G
First Dynode	(27.64, 62.98) in	(490, 27) G	(444, 209) G
Middle Dynode	(28.54, 65.30) in	(416, 221) G	(303, 361) G
Shield End #2	(29.57, 67.79) in	(342, 193) G	(245, 308) G

Table 1: Coordinates of a representative CTOF PMT of the high-pitch angle and the low-pitch angle designs positioned in the (y, z) plane in the CLAS12 global coordinate system. The associated field components are from a 3D field map of the CLAS12 solenoid. The positions are locations along the associated PMTs at the photocathode, the first dynode, and the middle of the accelerating structure, and at the faces of the heavy shield cones. The field components are given in the CLAS12 global coordinate system and in a primed coordinate system rotated with the z' axis along the shield symmetry axis.

Table 1 shows the field strength at the coordinate of the "Shield End #1" for the high-pitch angle design to be 1000 G and for the low-pitch angle design to be 1076 G. However, due to the different positions of the shields in the solenoid fringe field, the corresponding axial and transverse field components between the two designs are significantly different.

Our goal in setting up the shield tests in the FROST magnet fringe field was to attempt to reproduce the field profiles given in Table 1 for both the high-pitch angle design and the low-pitch angle design. As the measured field components were actually in a local coordinate system with the z' axis along the shield axis and the y' axis perpendicular to the shield axis with a rotation angle of θ_{high}=28° for the high-pitch angle design and θ_{low}=22° for the low-pitch angle design, we determined the primed field components $B_{y'}$ and $B_{z'}$ from the components B_y and B_z provided in Table 1 using the coordinate transformation:

$$B_{y'} = B_y \cos\theta - B_z \sin\theta \quad (1)$$

$$B_{z'} = B_y \sin\theta + B_z \cos\theta. \quad (2)$$

The field components that we are actually trying to match in the primed coordinate system are given in Table 1.

3.2 FROST Solenoid Field

The FROST magnet is a 5-T superconducting solenoid that has been used in Hall B to provide a high magnetic field for use with polarized target operation. At present the FROST magnet is setup in a dedicated test area in the Test Lab at JLab (see Fig. 6). The FROST magnet is 30-in long with a 5-in diameter bore (see Fig. 7).

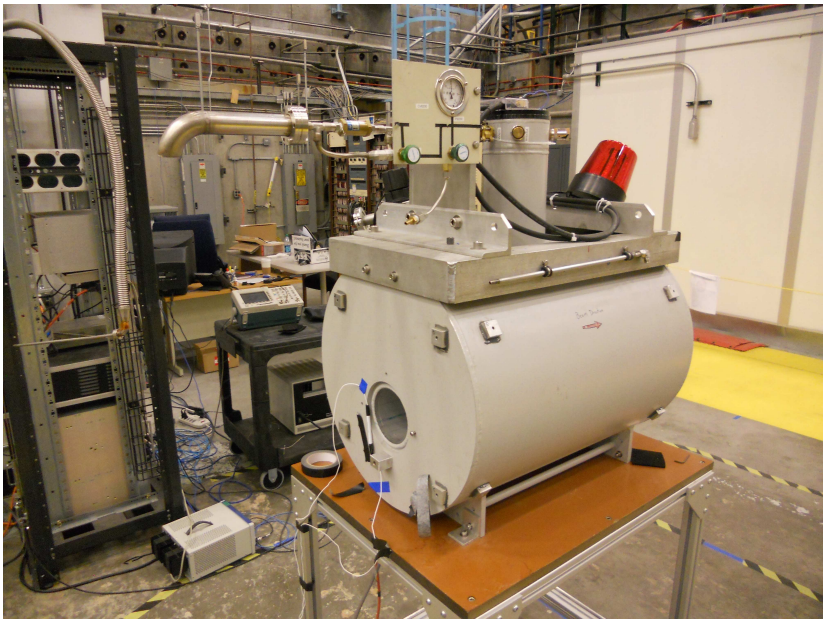

Figure 6: Photograph of the FROST magnet on its stand in the Test Lab at JLab.

Prior to using the magnet we had been provided with a set of field test measurements along the magnet's symmetry axis with which to normalize and adjust the field calculations. These data indicated that the field at the face of the magnet was ∼3 T. We found out shortly after energizing the magnet to full current (i=81.18 A) that the field at the face of the magnet on the symmetry axis was, in reality, only 2.2 kG.

The first step in our test plan was to measure the FROST magnet fringe field over a rather coarse grid of points to check the magnetic field map that had been generated. It was during this process that we found that the true fringe field of the magnet was significantly lower that we had been led to believe. However, it was still sufficient for our purposes. We simply had to map out the fields on the fly to determine where to position our shields for the tests.

All of the field measurements that were made employed a Metrolab 7025 3D Hall B (see Fig. 8). The hand-held base unit was equipped with a 3-ft-long cable attached to the probe itself. The probe included labels indicating its three coordinate axis directions, which were lined up to agree with our coordinate definitions along either the (x, y, z) or (x', y', z') axes depending on the measurement. The unit had its own LCD display but we employed the

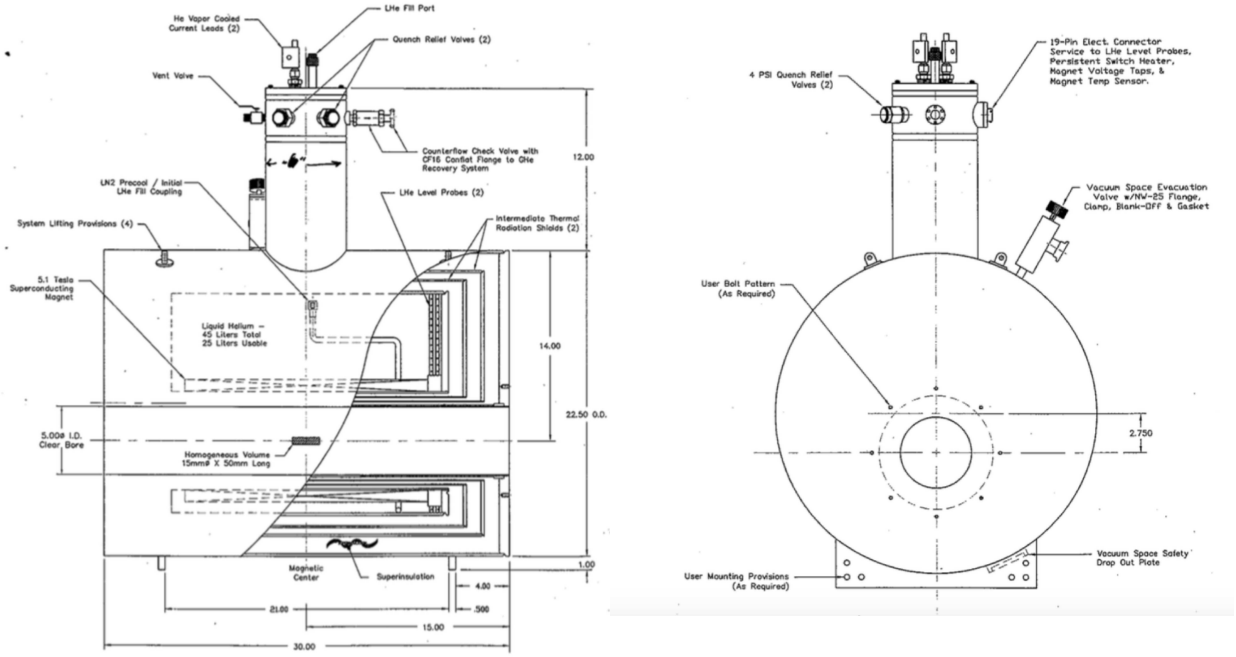

Figure 7: (Left) Side view and (right) end view schematic diagrams of the 5-T FROST superconducting solenoid magnet. The magnet is 30-in long with a 5-in diameter bore.

Figure 8: (Left) Photograph of the Metrolab 7025 3D Hall probe used for the magnetic field measurements. (Right) The user computer interface for the 3D Hall probe that allowed for the probe to be zeroed and for the three field components and the field magnitude to be measured.

included ancillary cable that connected to our laptop to read out the device. All data were recorded in our test EXCEL database.

Figure 9: Photograph of the fixture to measure the FROST magnet fringe field. Each of the 3 horizontal arms included three fiducial guides to position the 3D Hall probe for a field measurement as a function of (x, y). The fixture was then moved along a line parallel to the axis of the magnet to change z.

Fig. 9 shows our field mapping grid fixture. The grid included 9 positioning guides for the Hall probe at x= -9, 0, 9 in and y= -9, 0, 9 in, and the fixture was positioned at z=0.0, 25.0, 50.0 cm (at i=50.0 A) and at z=44.5, 50.0 cm (at i=81.18 A). The measurements at reduced magnet current (i=50.0 A) were taken as the Hall probe had a maximum field rating of 200 mT = 2000 G. To determine the field at full current, we simply scaled by the ratio of the currents (i.e. a factor of 81.18/50.0). The measured data are provided in Table 2. Note that the Hall probe was re-zeroed/re-calibrated after each time it was powered on, following the manufacturer's instructions.

The next step in our test plan was to find the coordinates in the fringe field that best matched the fields expected at the ends of the high-pitch angle shield and the low-pitch angle shield in the CLAS12 solenoid as given in Table 1. For this determination we used the support stand setup shown in Fig. 10. The angle of the shield support rail within the stand was adjustable over a reasonable range and the height of the support stand was set with shimming blocks. On the support rail a "dummy" shield cart was attached that contained an aluminum cylinder of the same diameter as the mandrel within the production shield. The cart could be positioned anywhere along the support rail. The positioning of the aluminum cylinder relative to the cart was set to be identical to that for the mandrel within the CTOF shield mounted on its own cart.

Our procedure for setting the position of the shields within the fringe field was to find the appropriate positions using the dummy shield cart fitted only with the aluminum cylinder.

Grid Measured at z=0				
(x, y)	B_x	B_y	B_z	B
(in)	(mT)	(mT)	(mT)	(mT)
(-9,9)	54.07	42.21	-26.69	73.60
(0,9)	4.12	92.71	-65.43	113.55
(9,9)	-40.10	51.31	-26.79	70.41
(-9,0)	96.28	-6.75	-74.36	121.84
(0,0)	-12.18	8.41	-250.20	250.63
(9,0)	-95.95	6.43	-70.46	119.22
(-9,-9)	53.42	-53.58	-38.32	84.81
(0,-9)	-0.84	-101.15	-85.40	132.38
(9,-9)	-54.07	-44.32	-31.82	76.81
Grid Measured at z=25 cm				
(x, y)	B_x	B_y	B_z	B
(-9,9)	16.41	10.94	-21.37	29.08
(0,9)	1.49	15.59	-33.77	37.22
(9,9)	-12.44	13.46	-23.79	30.03
(-9,0)	19.14	-3.56	-30.20	35.93
(0,0)	-0.73	-0.50	-48.06	48.07
(9,0)	-17.75	-0.50	-32.31	36.87
(-9,-9)	-14.89	-14.11	-22.42	30.39
(0,-9)	1.56	-19.40	-31.50	37.03
(9,-9)	-14.14	-14.08	-22.68	30.21
Grid Measured at z=50 cm				
(x, y)	B_x	B_y	B_z	B
(-9,9)	4.35	3.96	-11.28	12.73
(0,9)	-0.54	4.25	-13.57	14.23
(9,9)	-4.50	4.37	-10.96	12.63
(-9,0)	5.08	-0.81	-13.41	14.36
(0,0)	-0.54	-0.39	-16.24	16.25
(9,0)	-5.10	-0.10	-13.43	14.36
(-9,-9)	4.03	-4.77	-11.51	13.10
(0,-9)	-0.08	-5.59	-13.43	14.54
(9,-9)	-4.82	-4.95	-11.35	13.29

Table 2: FROST magnet fringe field data measured at z coordinates relative to the face of the magnet of z=0, 25, 50 cm. The z axis is along the solenoid axis, the y axis is perpendicular to the floor, and the x axis is horizontal to the floor. Note that these data were measured with a reduced magnet current of i=50.0 A and scaled to the full-current field setting of i=81.18 A.

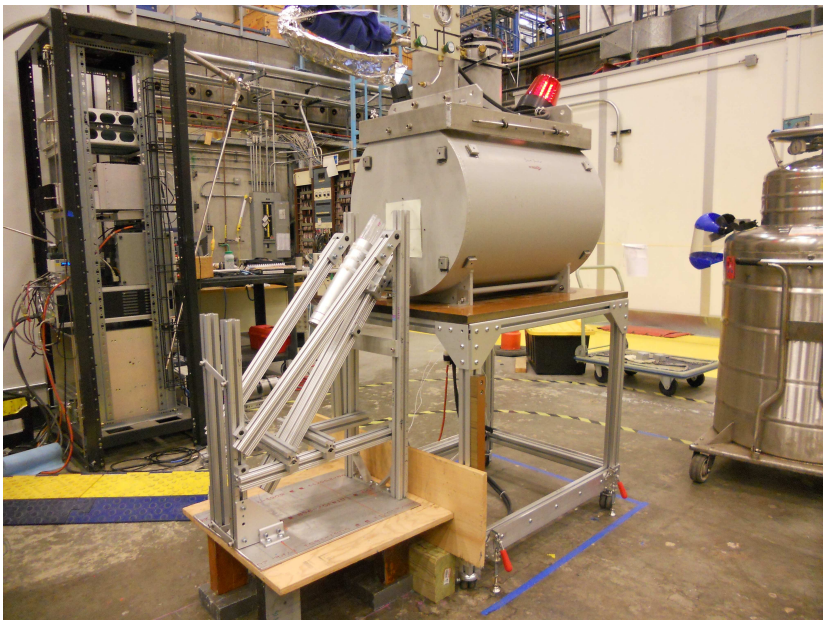

Figure 10: Photograph of the setup to determine the shield positioning within the FROST magnet fringe field.

Once the appropriate field conditions were found, we would then replace the dummy shield cart with the cart outfitted with the test shield. For both carts at a given location along the support rail, the mandrels would be in the same exact position to mm-level tolerances.

Fig. 11 shows a close-up of the dummy cart outfitted with the aluminum cylinder. Within the cylinder were mounted three parallel plastic tubes that each defined an axis into which the Hall probe could be inserted. The Hall probe was marked with five depth positions based on the known CTOF shield and PMT geometries such that when it was inserted into a given tube, we could measure the field at z' positions corresponding to:

- Shield End #1
- Photocathode
- First Dynode
- Middle Dynode
- Shield End #2

Our measurements of the FROST magnet fringe fields at these locations for the high-pitch angle shield position and for the low-pitch angle shield position are given in Tables 3 and 4, respectively. Note that for all measurements the field data were recorded with the 3 plastic tubes parallel to the cart support rail and rotated by 90° so all 3 tubes were in the same vertical plane. Note that locating the coordinates to position the shield cannot be done with the shield in place because its very presence modifies the fringe field distribution and it also blocks access to position the Hall probe.

High-Pitch Angle Design (Units = mT)								
Position	$B_{x'}$	$B_{y'}$	$B_{z'}$	B	$B_{x'}$	$B_{y'}$	$B_{z'}$	B
Shield End #1	-10.37	79.40	-64.80	103.01	27.00	46.90	-85.30	101.02
Shield End #2	-1.40	7.41	-23.50	24.68	-71.40	-22.50	-110.20	133.22
Horizontal Tube Orientation								
	Left Tube							
Ph Cath	-10.49	26.30	-44.70	52.91	0.01	0.00	-0.01	0.01
1st Dyn	-5.10	23.30	-41.30	47.69	0.01	-0.01	-0.01	0.02
Mid Dyn	-5.48	16.90	-35.40	39.61	0.01	-0.02	-0.02	0.03
	Middle Tube							
Ph Cath	-0.84	27.50	-45.00	52.74	0.01	0.00	-0.02	0.02
1st Dyn	-2.94	24.30	-41.60	48.27	0.00	-0.01	-0.02	0.02
Mid Dyn	-7.19	17.17	-35.30	39.91	0.01	-0.01	-0.03	0.03
	Right Tube							
Ph Cath	-8.08	28.00	-43.00	51.95	0.02	-0.01	-0.02	0.03
1st Dyn	-9.41	23.50	-40.10	47.42	0.02	0.00	-0.02	0.03
Mid Dyn	-7.53	17.60	-34.10	39.11	0.04	0.00	-0.03	0.05
Vertical Tube Orientation								
	Top Tube							
Ph Cath	-3.94	28.10	-40.70	49.61	0.02	-0.01	-0.04	0.05
1st Dyn	-4.91	23.50	-37.60	44.61	0.02	-0.02	-0.04	0.05
Mid Dyn	-3.94	17.80	-32.90	37.61	0.01	-0.02	-0.03	0.04
	Middle Tube							
Ph Cath	-7.23	27.00	-44.40	52.47	0.03	-0.03	-0.03	0.05
1st Dyn	-5.39	23.30	-41.20	47.64	0.03	-0.02	-0.02	0.04
Mid Dyn	-4.03	17.47	-35.70	39.95	0.02	-0.02	-0.05	0.06
	Bottom Tube							
Ph Cath	-4.15	28.00	-48.50	56.16	0.02	-0.02	-0.03	0.04
1st Dyn	-5.11	22.80	-44.70	50.44	0.02	-0.02	-0.02	0.03
Mid Dyn	-2.06	17.36	-38.20	42.01	0.03	-0.01	-0.02	0.04

Table 3: High Pitch-Angle: (Left) Measurements of the FROST magnet fringe field along the CTOF shield system in a field that best matched the configuration of the high-pitch angle shield in the fringe field of the CLAS12 solenoid. (Right) Measurements of the field within the CTOF shield system. (Compensation coils off)

Low-Pitch Angle Design (Units = mT)								
Position	$B_{x'}$	$B_{y'}$	$B_{z'}$	B	$B_{x'}$	$B_{y'}$	$B_{z'}$	B
Shield End #1	4.53	66.7	-84.3	107.59	46.20	38.00	-110.10	125.30
Shield End #2	-0.55	5.38	-22.3	22.95	-86.20	12.46	-114.20	143.62
Horizontal Tube Orientation								
	Left Tube							
Ph Cath	-6.40	20.40	-45.20	50.00	0.01	0.00	-0.01	0.01
1st Dyn	-1.22	18.14	-41.60	45.40	0.01	0.00	-0.01	0.01
Mid Dyn	0.25	13.20	-35.10	37.50	0.00	0.00	-0.01	0.01
	Middle Tube							
Ph Cath	-1.17	19.90	-46.20	50.32	0.01	0.01	-0.01	0.02
1st Dyn	0.21	17.23	-41.80	45.21	0.01	0.00	-0.01	0.01
Mid Dyn	-0.54	12.25	-35.00	37.09	0.01	0.00	-0.03	0.03
	Right Tube							
Ph Cath	-7.37	20.80	-46.70	51.65	0.00	0.00	-0.02	0.02
1st Dyn	-5.15	17.67	-42.00	45.86	0.01	0.00	-0.01	0.01
Mid Dyn	-3.86	13.00	-35.40	37.91	0.03	0.01	-0.03	0.04
Vertical Tube Orientation								
	Top Tube							
Ph Cath	1.66	21.20	-43.80	48.69	0.02	0.00	-0.03	0.04
1st Dyn	0.17	18.22	-39.70	43.68	0.02	0.00	-0.03	0.04
Mid Dyn	0.27	13.49	-33.20	35.84	0.01	0.00	-0.04	0.04
	Middle Tube							
Ph Cath	-2.34	20.30	-47.10	51.34	0.02	0.00	-0.03	0.04
1st Dyn	-1.53	16.93	-42.40	45.68	0.02	0.00	-0.03	0.04
Mid Dyn	0.54	12.17	-35.20	37.25	0.02	0.00	-0.03	0.04
	Bottom Tube							
Ph Cath	-1.74	19.70	-50.50	54.23	0.03	0.00	-0.02	0.04
1st Dyn	1.08	16.34	-45.20	48.07	0.03	0.00	-0.02	0.04
Mid Dyn	0.21	12.01	-37.50	39.38	0.04	0.01	-0.02	0.05

Table 4: Low Pitch-Angle: (Left) Measurements of the FROST magnet fringe field along the CTOF shield system in a field that best matched the configuration of the low-pitch angle shield in the fringe field of the CLAS12 solenoid. (Right) Measurements of the field within the CTOF shield system. (Compensation coils off)

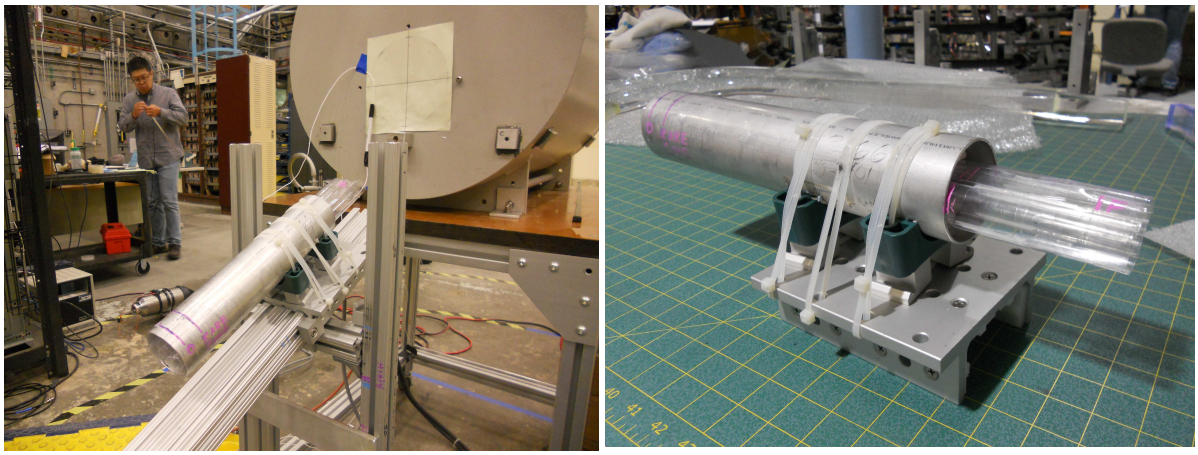

Figure 11: Close-up photographs of the setup used to determine the shield placement within the FROST magnet fringe field. Within the aluminum cylinder were three plastic tubes that accepted the 3D Hall probe and allowed for measurements at the locations outlined in Table 1. The measurements were recorded at positions along the central axis of the PMT and along axes against the inner surface of the inner shield. The 3 tubes could be rotated such that measurements could be carried out with the tubes oriented in a vertical plane and a horizontal plane relative to the aluminum tube.

Once the dummy cart setups and positions were determined to place the shield in fields similar to those expected in the CLAS12 solenoid fringe field, the dummy cart was taken off the rail and replaced with the production shield for testing.

4 Shield Test Plan

4.1 Nominal Field Studies

The test plan amounted to measuring the internal remnant fields within the CTOF magnetic shield in positions that well matched those for the high-pitch angle design and low-pitch angle design. For the measurements the PMT was removed and replaced with a tube system just as was designed for the dummy shield cart within the aluminum cylinder. Three plastic tubes were inserted that could be positioned with all 3 tubes parallel to the support rail or so that they were all in the same vertical plane. Then the field components along each tube were measured at locations that matched the locations of the PMT photocathode, first dynode, and the middle of the accelerating structure. Figs. 12 and 13 show the two nominal shield configurations and cart setups.

4.1.1 Effect of Passive Shield Layers with Nominal External Fields

Table 3 shows the data measured for the high-pitch angle design positioning and Table 4 shows the data measured for the low-pitch angle design positioning. Initially all data were recorded with the compensation coils turned off. Note that the data was measured in the

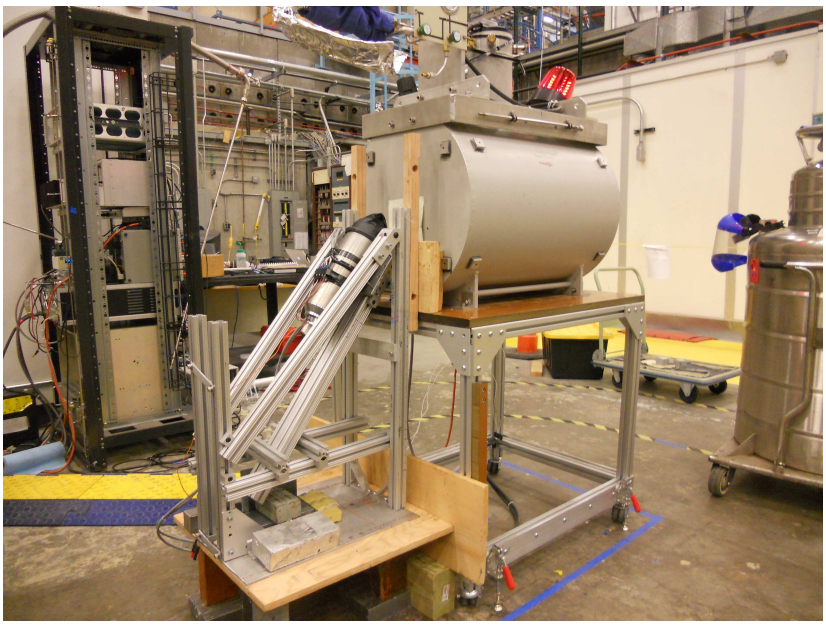

Figure 12: Photograph of the CTOF magnetic shield in the FROST magnet fringe field at positioned at a location that produced a field magnitude and gradient consistent with the high-pitch angle shield positioning in the CLAS12 solenoid fringe field.

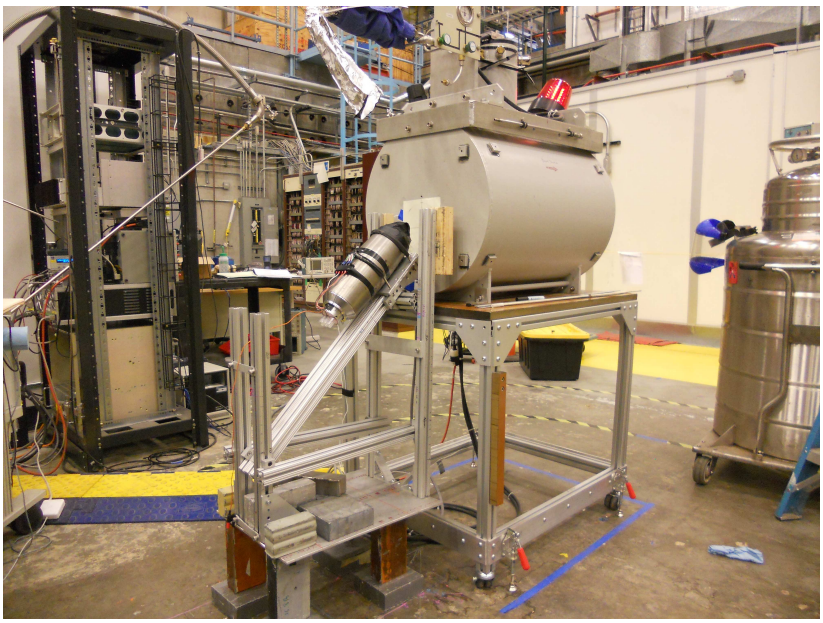

Figure 13: Photograph of the CTOF magnetic shield in the FROST magnet fringe field at positioned at a location that produced a field magnitude and gradient consistent with the low-pitch angle shield positioning in the CLAS12 solenoid fringe field.

primed coordinate system with the z' axis along the shield axis and the y' axis perpendicular to this axis. Also the data on the left side of Tables 3 and 4 were measured using the dummy shield cart (no shield or magnetic elements present).

The data measured for the internal remnant fields based on a shielding system with only the three passive layers in Tables 3 and 4 clearly show the efficacy of the design. The basic findings include:

- All field components were measured to be less than 0.5 G at all positions along the PMT and for all axes measured in the horizontal and vertical tube orientations.
- The fields measured in the horizontal tube orientation measurements were typically a factor of two smaller than the fields measured in the vertical tube orientation which is a reasonable observation given that the shield layers are far from saturation. In the such a case the internal remnant field lines should match the direction of the external field lines. The azimuthal orientation of the PMT within the Co-NETIC layer takes this into account to minimize $\vec{v} \times \vec{B}$ effects that might otherwise result in loss of photoelectrons from the acceleration chain.
- The field components are reasonably uniform across the horizontal tube measurements and also across the vertical tube measurements.

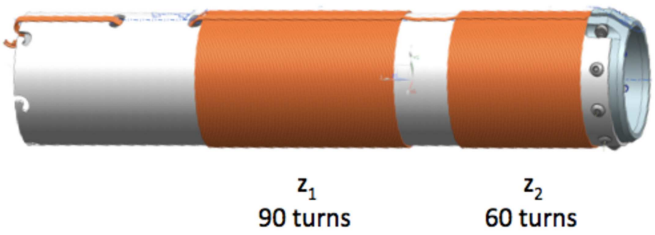

Figure 14: Model layout of the compensation coils on the shield mandrel showing the coil z_1 with 90 turns and coils z_2 with 60 turns. z_1 spans the middle to back part of the PMT dynode structure and z_2 spans the region about the PMT photocathode.

4.1.2 Compensation Coil Studies with Nominal External Fields

The next step in the shield test plan was to study the effect of the compensation coils on affecting the internal field along the PMT. The coils are called z_1 and z_2 and are illustrated in Fig. 14. The coil z_1 contains 90 turns and is positioned about the dynodes of the PMT accelerating structure. The coil z_2 contains 60 turns and is positioned about the PMT photocathode. Fig. 4 shows the relational positioning between the coils and the PMT in the 3D shield model. For these initial studies we employed the following coil current settings:

- $i_{z_1} = i_{z_2} = 0.5$ A
- $i_{z_1} = i_{z_2} = 0.75$ A

- $i_{z_1} = i_{z_2} = 1.0$ A,

with the shield in its nominal low-pitch angle position relative to the FROST magnet. This grid was reasonably limited due to the already low internal fields in this configuration. A more extensive set of current settings was studied during the shield stress tests in Section 4.2.

The low voltage power supply for the CTOF compensation coils is a Weiner MPOD mini-crate outfitted with two modules. Each module has 8 channels that can individually provide up to 50 W per channel with a maximum current of 5 A. The connections of the wiring harness to the shield system are shown in Fig. 15. For these tests the power supply was connected to the compensation coil leads through 50-ft-long power cables. For the CTOF configuration, the coils z_1 and z_2 are independently controllable. The MPOD system is controlled through the vendor supplied interface shown in Fig. 16.

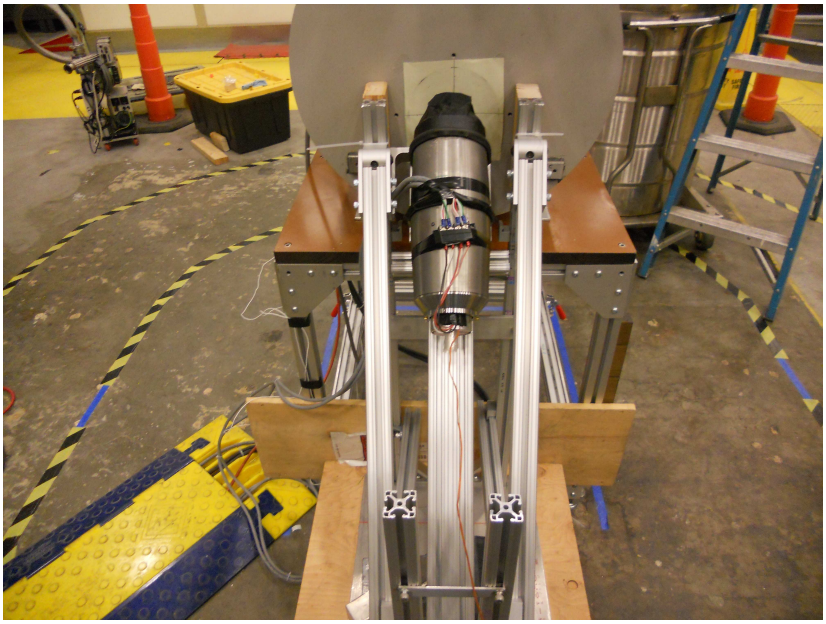

Figure 15: End view of the CTOF magnetic shield in the FROST magnet fringe field showing the wiring harness used to power the two internal compensation coils.

For each current setting of the compensation coils, database tables of the form shown in Tables 3 and 4 were completed. The results with energizing the coils up to the level of 1 A are certainly not dramatic at these low currents. At 1 A, both coils produce a field of 10 G, however the Co-NETIC shield layer is inside the compensation coil layer and shields much of the created field. The data for the middle measurement tube (along the shield axis) is shown in Fig. 17.

The data shown in Fig. 17 represent only a portion of the recorded data. The interpretation of the setup using the compensation coils would be most straightforward if the trends for $B_{x'}$, $B_{y'}$, and $B_{z'}$ behaved similarly along all PMT tube axes measured, i.e. along the outer tubes in the different tube measurement configurations. That was not always found to be the case. Sometimes reducing the fields along the central tube gave rise to increased

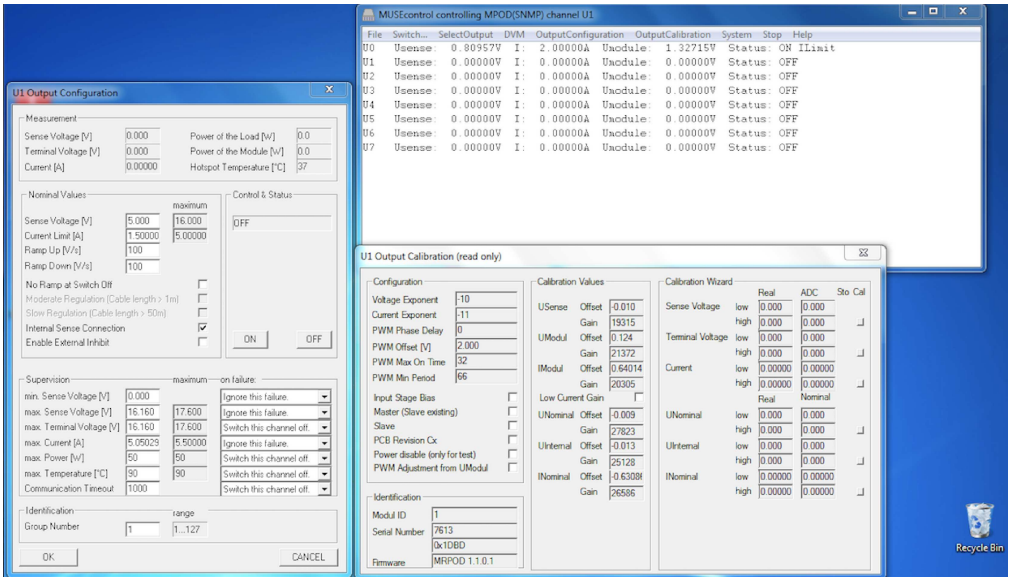

Figure 16: User interface to control the Weiner MPOD low voltage power supply used to power the compensation coils.

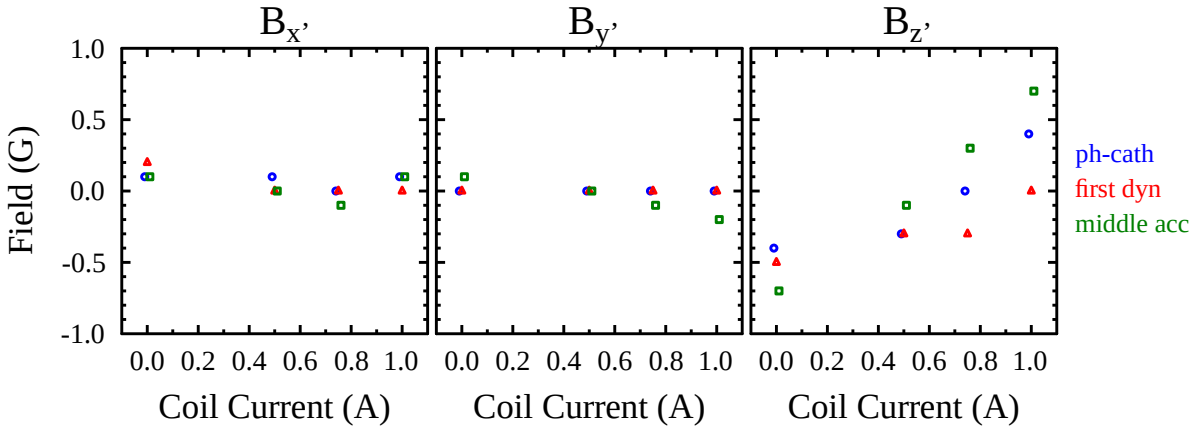

Figure 17: Low-Pitch Angle: Measured field components along the PMT in the middle measurement tube as a function of the compensation coil current. For these tests the currents were the same in z_1 and z_2. The different colored data points represent the different positions measured along the PMT position as indicated.

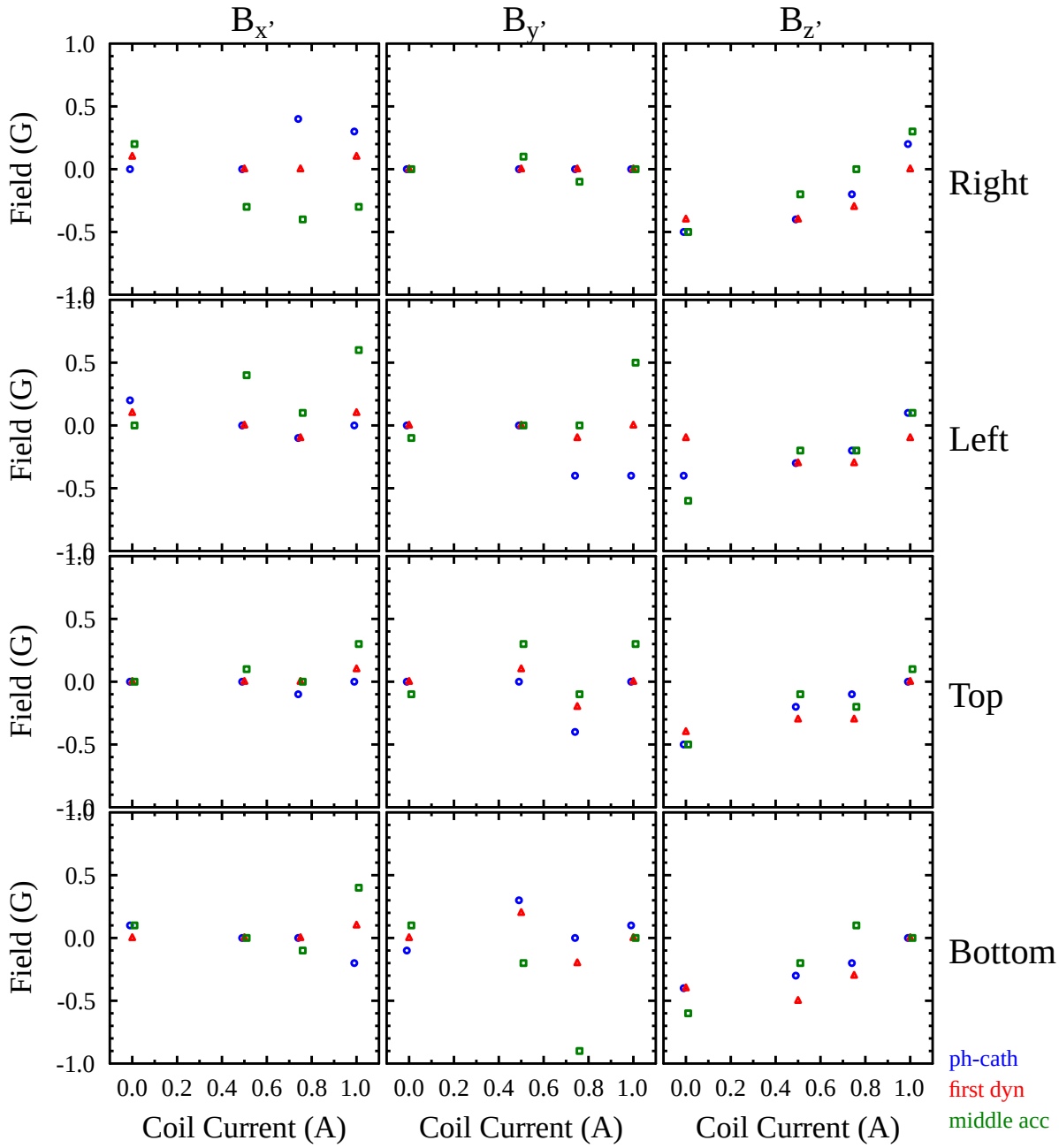

Figure 18: Low-Pitch Angle: Measured field components along the PMT in the outer measurement tubes as a function of the compensation coil current. For this test the currents were the same in z_1 and z_2. The different colored data points represent the different positions measured along the PMT position as indicated.

off-axis fields. Fig. 18 shows the recorded field data along the outer horizontal tubes and the outer vertical tubes.

While the effects of generating a small field with the compensation coils are reasonably subtle, these data as a whole reveal a few apparent trends:

- Increasing the current in z_1 and z_2 reduces the $B_{z'}$ component to zero and causes it to undergo a sign change between i=0.75 and 1.0 A.
- The $B_{x'}$ and $B_{y'}$ components are reasonably unaffected at the location of the photocathode and the first dynode, but show a reduction and then a zero crossing at the middle of the accelerating structure.
- The PMTs are oriented such that their performance is relatively insensitive to small fields in the y' direction. The goal of tuning the currents in the individual coils should be to minimize the fields in the x' direction to minimize any loss of photoelectrons due to $\vec{v} \times \vec{B}$ forces that will cause loss of photoelectrons and, therefore, gain.

Note also that a similar compensation coil current scan was completed for the shield in the high-pitch angle configuration with similar qualitative results and similar conclusions were drawn based upon the results.

4.2 Stress Test Field Studies

Our next phase of testing the shield performance was to reposition the shields in higher field locations closer to the face of the solenoid. To measure the fields relevant for the shield placement, we once again installed the dummy shield cart with the aluminum cylinder on the support rail. Four higher field configurations were studied. The field configurations into which the shield was positioned are detailed in Tables 5 to 7. Again the fringe field measurements on the left-side of these data tables were made with the cart outfitted with only the aluminum cylinder.

4.2.1 Effect of Passive Shield Layers in Higher Fields

Examining the measurements from Stress Test #1 to Stress Test #3 shown in Tables 5 to 7, which positioned the CTOF shield in fields at the face closest to the magnet 30% to 200% higher than the nominal expected value, while varying both the axial and transverse field components seen by the shield, the performance is quite good over the broad range of these test conditions. For Stress Test #3, the maximum internal remnant field without the compensation coil energized was typically well less than 1 G, with maximum readings below 1.5 G.

For the Stress Test #1 data, we see that the field components measured in the vertical tube orientation are larger than for those measured in the horizontal tube orientation. This is quite similar to the findings for the nominal high-pitch angle and low-pitch angle shield studies (see Section 4.1). However, the results for Stress Test #2 and Stress Test # show much more consistency between the field components measured in the horizontal tube orientation and the vertical tube orientation. For these studies the peak field at the end of the

(Units = mT)	Fringe Fields				Internal Fields			
Position	$B_{x'}$	$B_{y'}$	$B_{z'}$	B	$B_{x'}$	$B_{y'}$	$B_{z'}$	B
Shield End #1	-16.03	100.70	-97.9	141.36	-58.50	71.40	-162.50	186.89
Shield End #2	-1.97	8.33	-26.7	28.04	3.29	-96.30	-125.40	158.14
Horizontal Tube Orientation								
	Left Tube							
Ph Cath	4.00	32.00	-55.30	64.02	0.03	0.00	-0.01	0.03
1st Dyn	4.11	26.40	-50.10	56.78	0.02	0.00	0.00	0.02
Mid Dyn	2.67	19.90	-42.30	46.82	0.00	0.00	-0.02	0.02
	Middle Tube							
Ph Cath	-6.30	30.50	-56.70	64.69	0.01	0.00	0.02	0.02
1st Dyn	-1.21	25.80	-51.50	57.61	0.00	-0.01	0.00	0.01
Mid Dyn	-1.57	18.50	-42.70	46.56	0.00	-0.02	-0.04	0.04
	Right Tube							
Ph Cath	-9.60	29.90	-57.10	65.17	0.01	0.00	-0.01	0.01
1st Dyn	-8.99	25.10	-51.50	57.99	0.02	-0.01	-0.01	0.02
Mid Dyn	-8.55	18.10	-42.90	47.34	0.04	0.00	-0.03	0.05
Vertical Tube Orientation								
	Top Tube							
Ph Cath	5.32	31.30	-52.80	61.61	0.03	0.00	-0.03	0.04
1st Dyn	-2.50	26.10	-47.90	54.61	0.03	-0.01	-0.02	0.04
Mid Dyn	-2.56	18.90	-40.50	44.77	0.02	-0.02	-0.03	0.04
	Middle Tube							
Ph Cath	-0.22	30.70	-57.60	65.27	0.03	-0.01	-0.04	0.05
1st Dyn	-1.61	25.00	-52.50	58.17	0.02	-0.01	-0.03	0.04
Mid Dyn	-3.54	18.18	-43.60	47.37	0.02	-0.01	-0.07	0.07
	Bottom Tube							
Ph Cath	0.13	29.40	-62.70	69.25	0.03	-0.03	-0.04	0.06
1st Dyn	2.53	23.80	-56.50	61.36	0.01	-0.01	-0.03	0.03
Mid Dyn	1.14	17.52	-46.50	49.70	0.01	0.01	-0.04	0.04

Table 5: Stress Test #1. (Left) Measurements of the FROST magnet fringe field along the CTOF shield system in a field configuration whose peak fields are larger than those expected in the fringe field of the CLAS12 solenoid. (Right) Measurements of the fields within the CTOF shield system in this fringe field. (Compensation coils off)

(Units = mT)	Fringe Fields				Internal Fields			
Position	$B_{x'}$	$B_{y'}$	$B_{z'}$	B	$B_{x'}$	$B_{y'}$	$B_{z'}$	B
Shield End #1	-42.70	132.50	-109.20	176.93	63.90	101.50	-183.40	219.14
Shield End #2	-1.54	11.42	-30.40	32.51	-106.50	-2.78	-169.30	200.03
Horizontal Tube Orientation								
	Left Tube							
Ph Cath	-20.50	40.00	-67.10	80.76	-0.04	-0.06	0.06	0.09
1st Dyn	-18.00	33.40	-61.70	72.43	-0.08	-0.07	0.08	0.13
Mid Dyn	-14.19	23.70	-52.90	59.68	-0.10	-0.06	0.07	0.14
	Middle Tube							
Ph Cath	-7.07	42.70	-68.80	81.28	-0.01	-0.07	0.03	0.08
1st Dyn	-2.07	36.00	-63.80	73.29	-0.09	-0.07	0.08	0.14
Mid Dyn	-3.50	24.60	-52.60	58.17	-0.10	-0.07	0.05	0.13
	Bottom Tube							
Ph Cath	-14.03	42.60	-68.90	82.21	-0.11	-0.05	0.06	0.13
1st Dyn	-12.74	35.40	-63.50	73.81	-0.09	-0.06	0.09	0.14
Mid Dyn	-9.72	25.10	-52.90	59.35	-0.08	-0.07	0.06	0.12
Vertical Tube Orientation								
	Top Tube							
Ph Cath	-24.60	35.80	-62.10	75.78	-0.01	-0.04	0.06	0.07
1st Dyn	-26.40	24.50	-56.70	67.17	-0.09	-0.05	0.08	0.13
Mid Dyn	-18.50	19.20	-48.40	55.26	-0.09	-0.08	0.07	0.14
	Middle Tube							
Ph Cath	1.16	40.60	-68.50	79.64	-0.08	-0.05	0.04	0.10
1st Dyn	-5.47	32.50	-61.70	69.95	-0.08	-0.05	0.07	0.12
Mid Dyn	-4.94	22.70	-52.10	57.04	-0.08	-0.05	0.05	0.11
	Right Tube							
Ph Cath	-1.72	40.20	-75.50	85.55	-0.10	-0.08	0.05	0.14
1st Dyn	-5.87	31.10	-66.30	73.47	-0.09	-0.06	0.07	0.13
Mid Dyn	-6.62	21.00	-55.70	59.89	-0.09	-0.03	0.05	0.11

Table 6: Stress Test #2. (Left) Measurements of the FROST magnet fringe field along the CTOF shield system in a field configuration whose peak fields are larger than those expected in the fringe field of the CLAS12 solenoid. (Right) Measurements of the fields within the CTOF shield system in this fringe field. (Compensation coils off)

(Units = mT)	Fringe Fields				Internal Fields			
Position	$B_{x'}$	$B_{y'}$	$B_{z'}$	B	$B_{x'}$	$B_{y'}$	$B_{z'}$	B
Shield End #1	-19.07	123.20	-182.40	220.93	71.90	83.00	-216.00	242.31
Shield End #2	-0.88	6.85	-30.13	30.92	-115.00	4.99	-176.60	210.80
Horizontal Tube Orientation								
	Left Tube							
Ph Cath	12.49	24.93	-80.80	85.48	0.04	0.00	0.01	0.04
1st Dyn	10.96	18.64	-70.93	74.16	-0.03	-0.01	0.04	0.05
Mid Dyn	4.63	13.60	-57.20	58.98	-0.08	-0.03	0.04	0.09
	Middle Tube							
Ph Cath	-4.41	42.53	-81.60	92.13	-0.04	-0.07	-0.09	0.12
1st Dyn	-1.79	21.67	-69.73	73.04	-0.05	-0.04	0.03	0.07
Mid Dyn	-0.84	15.29	-55.47	57.54	-0.06	-0.04	0.00	0.07
	Right Tube							
Ph Cath	-9.33	29.20	-79.47	85.17	-0.08	-0.12	0.00	0.14
1st Dyn	-7.19	23.43	-69.47	73.66	-0.06	-0.05	0.04	0.09
Mid Dyn	-5.65	16.07	-54.40	57.00	-0.03	-0.02	0.02	0.04
Vertical Tube Orientation								
	Top Tube							
Ph Cath	-0.84	28.27	-73.87	79.09	-0.07	0.03	0.00	0.08
1st Dyn	2.04	22.44	-65.33	69.11	-0.07	-0.02	0.05	0.09
Mid Dyn	-0.80	16.21	-52.67	55.11	-0.07	-0.08	0.04	0.11
	Middle Tube							
Ph Cath	0.76	27.20	-79.60	84.12	-0.06	-0.05	-0.04	0.09
1st Dyn	0.88	21.03	-69.60	72.71	-0.08	-0.04	0.04	0.10
Mid Dyn	1.53	14.27	-55.20	57.03	-0.08	-0.05	0.00	0.09
	Bottom Tube							
Ph Cath	-1.53	24.40	-85.07	88.51	-0.08	-0.12	0.00	0.14
1st Dyn	-2.48	19.45	-74.93	77.46	-0.06	-0.05	0.05	0.09
Mid Dyn	-3.19	12.97	-58.13	59.65	-0.06	-0.02	0.02	0.07

Table 7: Stress Test #3. (Left) Measurements of the FROST magnet fringe field along the CTOF shield system in a field configuration whose peak fields are larger than those expected in the fringe field of the CLAS12 solenoid. (Right) Measurements of the fields within the CTOF shield system in this fringe field. (Compensation coils off)

shield tube near the face of the magnet is roughly a factor of two larger than the nominal shield design value. In such a configuration the shield layers are much closer to a saturation condition and this begins to alter the predominant orientation of the inner remnant fields so they it no longer matches that of the external field lines.

4.2.2 Effect of Compensation Coils in Higher Fields

For the configuration labeled as "Stress Test #1", we again studied the effect of the compensation coil settings on reducing the now slightly larger internal remnant field components. For these studies, the current settings for z_1 and z_2 were scanned when they were set equal to each other (see Fig. 19) and for independent current settings of the two coils (see Fig. 20). The data shown in Figs. 19 and 20 are for the measurement tube along the PMT axis. Data for the other tubes (top, bottom, left, right) were also recorded and allowed for similar observations as were seen in Fig. 18, and thus are not shown. For the data shown here similar conclusions can be made regarding the trends as made in Section 4.1.2. Again the final current settings of the coils z_1 and z_2 will have to be determined in-situ after installation into the CLAS12 solenoid. However, it is clear that even in slightly elevated external magnetic fields compared to expectations that the coils can serve to reduce the internal remnant fields along the PMT to a level below 0.5 G as desired.

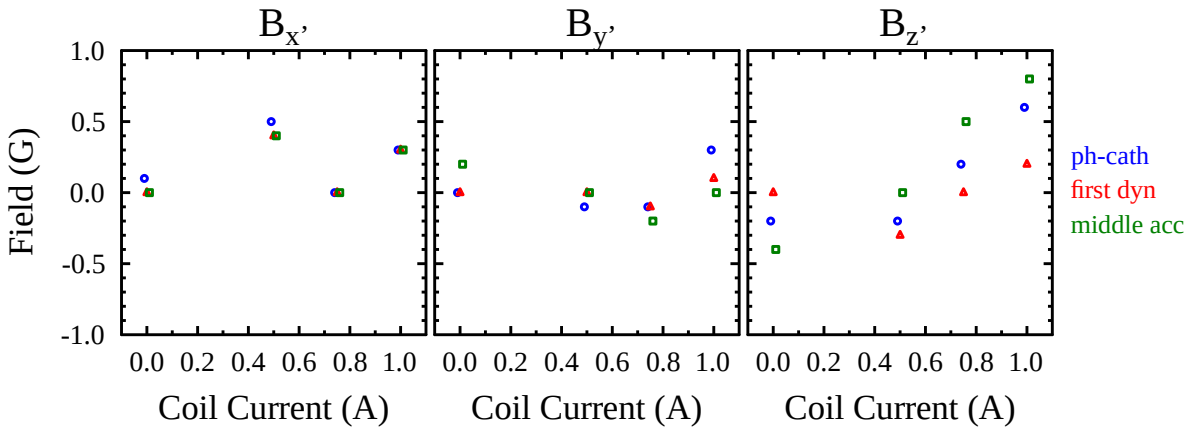

Figure 19: Stress Test #1: Measured field components along the PMT in the middle measurement tube as a function of the compensation coil current. For these tests the currents were the same in z_1 and z_2. The different colored data points represent the different positions measured along the PMT position as indicated.

5 Additional Compensation Coil Studies

5.1 Inner Fields

In order to better understand the shielding effect of the inner Co-NETIC cylinder on the field generated when energizing the compensation coils, a set of measurements of the field within the Co-NETIC cylinder (still contained within the full shield assembly) were carried

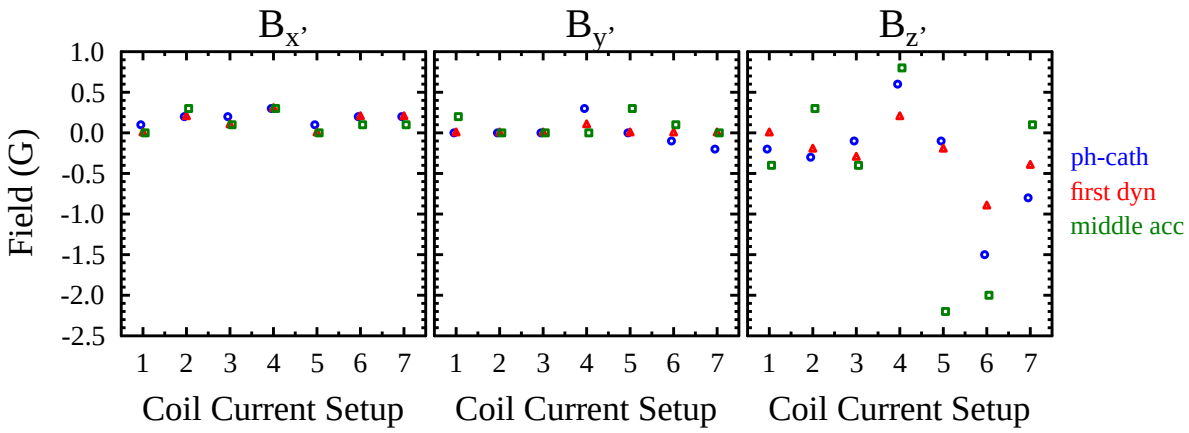

Figure 20: Stress Test #1: Measured field components along the PMT in the middle measurement tube as a function of the compensation coil current. For these tests the currents were set differently in z_1 and z_2. The different measurements correspond to: Point #1: z_1=0 A, z_2=0 A, Point #2: z_1=0.75 A, z_2=0 A, Point #3: z_1=0 A, z_2=0.75 A, Point #4: z_1=1 A, z_2=1 A, Point #5: z_1=-1 A, z_2=1 A, Point #6: z_1=-1 A, z_2=-1 A, Point #7: z_1=1 A, z_2=1 A. The different colored data points represent the different positions measured along the PMT position as indicated.

out on the bench after the tests with the FROST magnet had been completed. Note that at the start of these measurements we found the outer steel cylinder to be very weakly magnetized. Again data were recorded using the inserted tube system oriented with the tubes both horizontally and vertically mounted. For the inner tube along the central PMT axis, the measured data for the field components are shown in Fig. 21. For these data the currents in the coils z_1 and z_2 were set to be the same. Here the data show that the field component along the shield axis monotonically rises with increasing current in the coils as expected. Along the transverse axes, the field slightly increases with increasing current until i=1.0 A to 1.5 A before it begins to lessen. With further increase in current, the field along the x' and y' axis goes through zero and then changes sign and grows. However up to i=2.5 A, the transverse fields remain below 0.5 G.

5.2 Temperature Measurements

The final measurements reported here were to record the temperature at the surface of the coils as a function of the coil current. For these measurements a Fluke 80KB-A integrated DMM temperature probe was employed. This system provides a type-K thermocouple on one end of a 39-in-long lead with a standard banana jack connector that plugs into a Fluke DMM. The Fluke DMM includes a setting to read the temperature of the probe. The probe was attached to the middle of the long coil z_1 during the initial shield assembly. Temperatures were recorded every 30 s for about 4 hours. The current settings in the two coils were set to be the same for these studies at values of i=1.0, 2.0, 3.0, and 4.0 A. The current setting was increased when the temperatures began to approach equilibrium at the probe location. Fig. 22 shows the measured data at the four current settings. The expected equilibrium

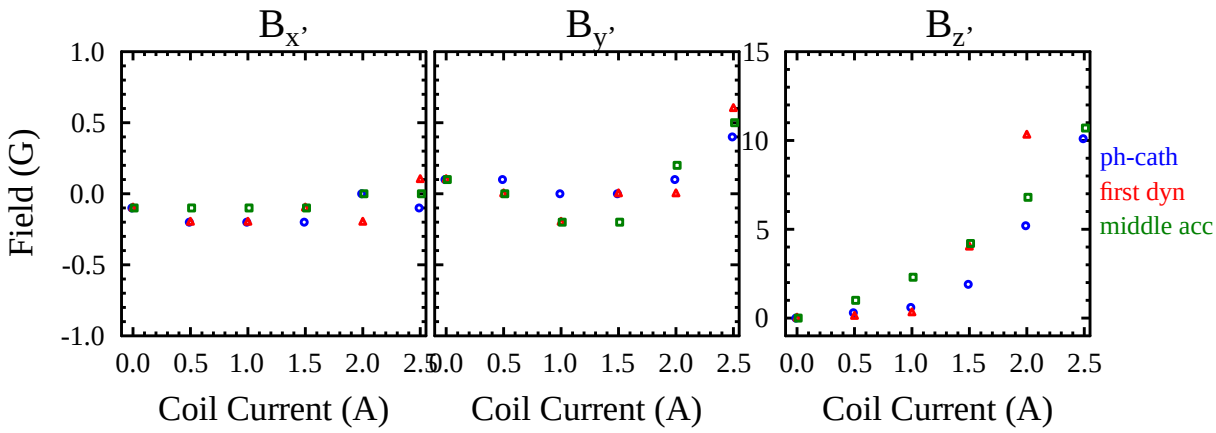

Figure 21: Bench Testing: Measured field components along the PMT in the middle measurement tube on the test bench in the CTOF lab as a function of the compensation coil current. For these tests the currents were the same in z_1 and z_2. The different colored data points represent the different positions measured along the PMT position as indicated.

temperatures based on these data are given in Table 8. Note that the limits given here are only crude estimates given the sizable thermal mass the shields actually present. Although the Weiner MPOD system can provide up to 5 A per channel, our findings from Section 4.1.2 showed that typical coil currents at the level of 0.75 A to 1.0 A were appropriate for shield operation. In this current regime the coil system remains at room temperature. During operation of the coil power supply in Hall B, appropriate operating current limit interlocks will be employed.

Current Setting	Temperature Limit
1 A	75 °F
2 A	80 °F
3 A	90 °F
4 A	120 °F

Table 8: Extrapolated temperature upper limits for the CTOF shield system from the temperature vs. time data recorded in Fig. 22 as a function of the operating current. These limits were derived with the same currents for the coils z_1 and z_2.

6 Summary and Conclusions

Reviewing the data in Tables 3 and 4 shows that the shield design for the passive layers meets all of its nominal design requirements. The internal remnant fields along the length of the PMT cavity for both the high-pitch angle and low-pitch angle designed are below 1 G everywhere. The fields at the photocathode, first dynode, and the middle of dynode accelerating structure well match the expectations from the detailed calculations shown in

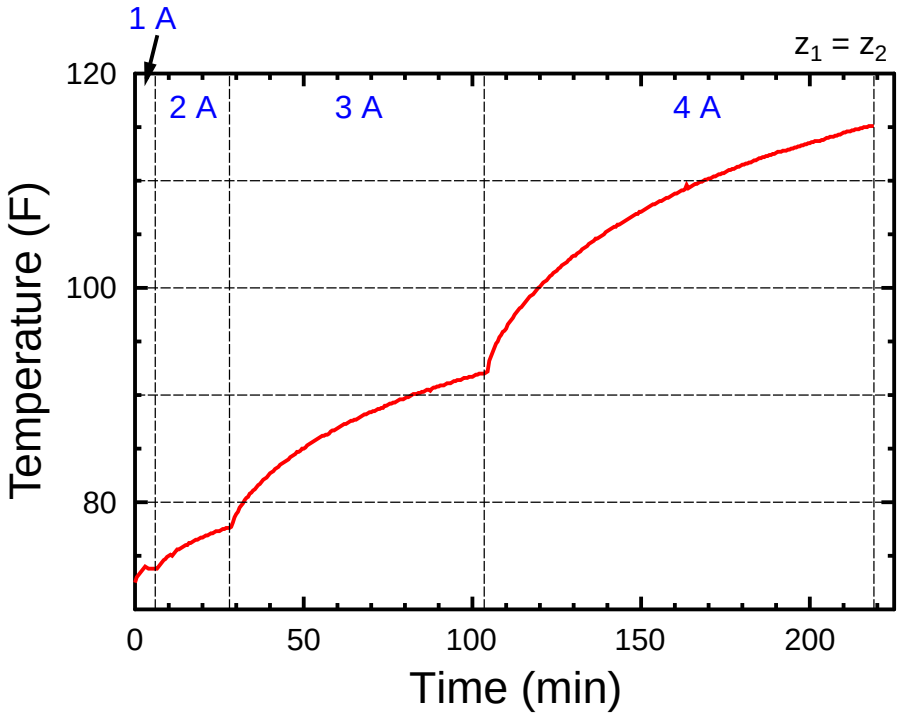

Figure 22: The measured coil temperature vs. time with the coils z_1 and z_2 energized to 1.0 A, 2.0 A, 3.0 A, and 4.0 A.

Fig. 2. The studies further indicate that the compensation coils can be operated with currents at the level of ∼1 A to bring the internal remnant fields down below 0.5 G.

Acknowledgments

Several folks provided wonderful assistance to us during these tests and we give our thanks for their efforts. Chris Keith instructed us on all phases of FROST magnet operation and provided regular and welcomed assistance throughout the week of the measurements. Renuka Rajput-Ghoshal provided the calculations for the field maps of the CLAS12 solenoid and the FROST solenoid, as well as the force calculations between the shield and the FROST magnet. Bob Miller is the lead CTOF project engineer and gave great advice during the setup of the tests. Cyril Wiggins is the lead CTOF project designer and assisted in extracting information from the design model as needed during these tests.

References

[1] V. Baturin and D.S. Carman, *Design and Performance Tests of the Dynamical Magnetic Shields for the CLAS12 Central Time-of-Flight Detector*, CLAS12-Note 2015-003.

[2] Opera 3-D magnetic field computations, see http://operafea.com/.